The Alpine thermo-tectonic evolution of the Aar and Gotthard massifs, Central Switzerland: Fission Track ages on zircon and apatite and K–Ar mica ages

by *Ingrid Michalski*[1] and *Michael Soom*[1,2]

Abstract

The Alpine uplift history of the Aar and Gotthard massifs since the Miocene has been constructed using 44 new fission track zircon and apatite analyses combined with Alpine ages published previously. From the gradient of fission track apatite age with sample elevation the palaeo-uplift rates have been calculated. During the last 2–4 Ma the fission track apatite ages were influenced through an uplift maximum near Brig and Chur. The minimum uplift region lies in the Reuss valley with a constant uplift rate of 0.5 mm/a during the last 10 Ma. From the transition zone of zircon pre-Alpine mixed ages (between Variscan cooling and Alpine cooling ages) to zircon Alpine cooling ages a temperature zone of 200° to at least 250 °C can be reconstructed. This temperature overprint of 200 to at least 250 °C is caused through very low grade Alpine metamorphism. The zircon cooling ages demonstrate an updoming of the complete Aar massif from east to west during Miocene.

Keywords: North- and Central Alps, Switzerland, K–Ar dating, fission track dating, metamorphism, uplift.

1. Introduction

In connection with the Swiss National Research Program NFP-20 on the "deep structure of Switzerland", new K–Ar and fission track (or ft) data in the Aar and Gotthard massifs have been obtained to extend the earlier results of WÜTHRICH, 1965; JÄGER et al., 1967; PURDY and JÄGER, 1976; SCHAER et al., 1975; WAGNER et al., 1977; FRANK and STETTLER, 1979; DEMPSTER, 1986 and SCHALTEGGER, 1986. The aim of the NFP 20 project was mainly a geophysical study. Since the interpretation of geophysical data gives only the present tectonic and thermal structure of the crust, radiometric age determinations represent a method by which the young tectonic and thermal history of a region can be reconstructed.

Because only a high sample density can lead to a detailed interpretation of the regional thermal and tectonic history it was necessary to combine new data of this study with ages published previously (WÜTHRICH, 1965; JÄGER et al., 1967; SCHAER et al., 1975; WAGNER, REIMER and JÄGER, 1977) (Fig. 1). Since STEIGER and JÄGER (1977), the international comparability of Rb–Sr and K–Ar data from different laboratories is generally accepted. In contrast, the comparability of ft results has been a contentious and confusing subject (HURFORD and GREEN, 1982, 1983). The lack of a uniquely quantified 238-U spontaneous fission decay constant and a multiplicity of techniques and conventions for assessing neutron fluence demands evaluation by each worker of their chosen parameters by analysis of materials regarded as age standards. Before directly comparing earlier ft ages of SCHAER et al. (1975) and WAGNER et al. (1977) with the new ft data of this study, it is the intention of this paper to verify their comparability.

A high ft apatite age density over the Aar and Gotthard massifs can show if the massifs are uplifted, for example, in one block or in several blocks, if they are tilted or if the uplift history was more complex. Ft length measurements in apatites can decipher in the low temperature range fast cooling, slow cooling and even reheating of a rock (GLEADOW et al., 1983).

[1] Laboratory for Isotope Geology, University of Bern, Erlachstrasse 9a, CH-3012 Bern, Switzerland.
[2] Present address: Geotest AG, Birkenstrasse 15, CH-3052 Zollikofen, Switzerland.
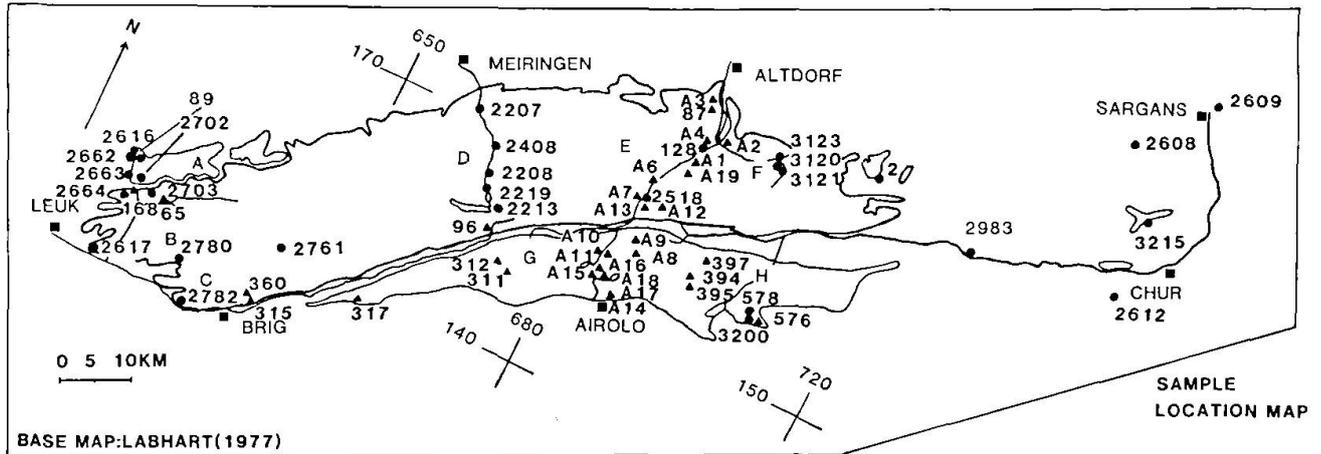
Fig. 1   Sample location map for the Aar- and Gotthard massif. The dots are new sample points, the triangles are sample points dated previously with the Rb–Sr, K–Ar and apatite ft method by WAGNER, REIMER and JÄGER (1977) and SCHAER et al. (1976). The capital letters represent the single regions which are discussed in the text. The coordinates are Swiss coordinates.

Since ft *zircon* analysis, with a closure temperature of 200–250 °C, represents the link between the ft apatite (120 °C closure temperature) and the K–Ar and Rb–Sr biotite (300 °C closure temperature) analysis the question arose whether the ft zircon ages can be related to the K–Ar and Rb–Sr biotite ages of the Aar and Gotthard massif (WÜTHRICH, 1965; JÄGER et al., 1967 and PURDY and JÄGER, 1976) or to the tectonic uplift history comparable to the ft apatite analysis.

2. Tectonic setting

The Variscan granites of the Aar and Gotthard massifs of Central Switzerland were intruded into a framework of different polymetamorphic pre-Variscan rocks. This basement, together with a Mesozoic sedimentary cover was deformed during Alpine orogeny and uplifted in late Tertiary time. The covering sediments were partly detached from the massifs to form the Helvetic nappes, whilst part of these sediments remained in contact with the crystalline basement (autochthonous/paraautochthonous). The erosion during the upper Miocene and Pliocene led to an exposure of the crystalline basement rocks. The lack of basement pebbles from the Aar massif in the Swiss Molasse basin seems to indicate that the basement of the Aar massif was not eroded before Tortonian times (i.e. during the last 10 Ma) (TRÜMPY, 1980). The grade of Alpine metamorphism in the massifs increases from north to south (Fig. 2). The northern parts of the Helvetic nappes show diagenesis; the border of the anchimetamorphism to the greenschist facies is defined at the northern edge of the Aar massif, whilst the transition zone from greenschist to amphibolite facies passes through the southern edge of the Gotthard massif (Fig. 1).

The Aar massif forms a huge dome of basements rocks covered or surrounded by Helvetic sediments. In the eastern part the massif plunges below its sedimentary cover and reappears north of Chur (Vättis basement window). From structural investigations the updoming of the Aar massif must be younger than the thrusting of the Helvetic nappes (PFIFFNER et al., 1988). There exist two geological models to explain the uplift of the Aar massif. BOYER and ELLIOTT (1982) consider the culmination of the massifs as a product of crustal shortening and thrusting of the massifs on the Alpine foreland. Alternatively NEUGEBAUER et al. (1980) discuss a general regional uplift during the Pliocene, due to isostatic reactions after the thrusting of the Helvetic nappes.

3. The geochronological framework

The concept of closure temperature is crucial for the understanding of radiometric data. DODSON (1973) offered the simple definition of closure temperature as being "the temperature of a system at the time represented by its apparent age". In essence the closure temperature of a mineral-isotope system represents a critical range above which the radiogenic daughter product is lost and below which the system is blocked against thermal disturbance, causing radiogenic products to accumulate. Estimations of closure temperature for the different radiogenic systems have been made from geological evidence and from laboratory experiments. WAGNER and REIMER (1972), PURDY and JÄGER
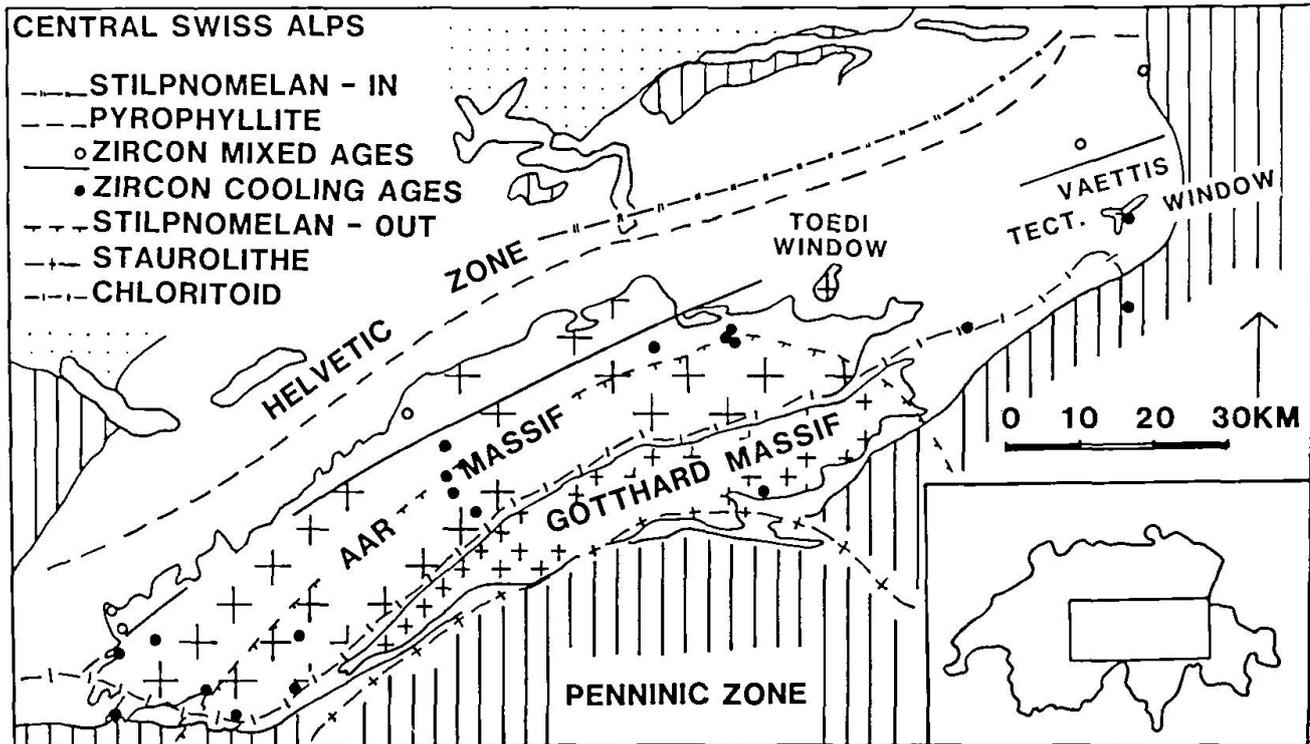
CENTRAL SWISS ALPS

—·—·— STILPNOMELAN - IN
— — — PYROPHYLLITE
———o ZIRCON MIXED AGES
——— • ZIRCON COOLING AGES
—·—·— STILPNOMELAN - OUT
—·+— STAUROLITHE
—·—·— CHLORITOID

HELVETIC ZONE

TOEDI WINDOW

VAETTIS TECT. WINDOW

AAR MASSIF   GOTTHARD MASSIF

0 10 20 30KM

PENNINIC ZONE

Fig. 2 The boundary between the zircon mixed age zone and the zircon cooling age zone in relation to the zones of Alpine metamorphism. Base map from FREY (1987).

(1976), WAGNER, REIMER and JÄGER (1977) and HURFORD (1986a) proposed the following closure temperatures from geological arguments: Rb–Sr muscovite (500 ± 50 °C) > K–Ar muscovite (350 ± 50 °C) > Rb–Sr biotite ≈ K–Ar biotite (300 ± 50 °C) > ft zircon (200 to 250 °C) > ft apatite (120 ± 20 °C).

Since the ft apatite method represents a low temperature geochronometer, its closure temperatures were essentially confirmed by direct observation of the age vs. temperature profile in deep drill holes (GLEADOW and DUDDY, 1981; LAKATOS and MILLER, 1983 and HAMMERSCHMIDT et al., 1984). For ft in apatite, extrapolation of the results of early laboratory annealing studies to geological time provided an estimate of ~100 °C for the closure temperature, below which tracks are effectively retained (WAGNER, 1968; NAESER and FAUL, 1969). Extrapolation to geological time of laboratory annealing experiments on zircon suggests effective closure temperatures > 300 °C (FLEISCHER et. al., 1965; KRISHNASWAMI et al., 1974) in stark contrast to geological evidence which favours a lower temperature between 200–250 °C (GLEADOW and BROOKS, 1979, HARRISON et al., 1979 and HURFORD, 1986b). Although no direct evidence is available to explain this difference it is conceivable that the cooling rate, activation energy and diffusion parameters may be contributory factors as well as fluid phases, chemistry and lattice defects.

With the reheating of a mineral in the temperature range of its closure temperature (the partial annealing zone) a so called "mixed" age would occur. Mixed ages can generally not be attributed to any geological event. Complete age resetting of a mineral depends on factors such as e.g. geochemical environment and mineral chemistry. Temperatures have to overshoot at least the closure temperature range of an isotope system over geological time spans.

Confined ft lengths in apatite and interpretation of measured ft age faciliate the diagnosis of the type of thermal history such as fast or slow steady cooling or even thermal overprinting (GLEADOW et al., 1983). Confined tracks lie parallel to the viewed surface and although totally enclosed within the crystal, intercept other outcropping tracks or fractures which faciliate the passage of etchant to the confined tracks (BHANDARI et al., 1971).

4. Methods

For *ft analyses* high purity concentrates of apatite and zircon were separated from each 15–30 kg sample using conventional crushing, Wilfley table and magnetic and heavy liquid techniques. *Apatites and zircons* were analysed using the external detector method (EDM) with spontaneous tracks being counted in the apatite and zircon crystals and induced tracks in an external detector of low uranium

mica, held in close contact with the crystals during irradiation. Apatites were mounted in Araldite, polished and etched in 5 N HNO$_3$ at 20 °C for 20 sec. Zircons were mounted in FEP-Teflon, polished and etched in a NaOH–KOH eutectic melt at 220 °C for 10–34 h (GLEADOW et al., 1976). Mica detectors were etched after irradiation to reveal induced tracks using 40% HF at 20 °C for 40 min. Track densities were determined using a Leitz Orthoplan microscope at a nominal magnification of 1250 using an oil-immersion objective. Only prismatic sections parallel to the c-crystallographic axis were used, having sharply etched polishing scratches and with well-etched tracks in all directions. For such crystals, a geometric factor of 0.5 is appropriate (GLEADOW and LOVERING, 1977; NAESER et al., 1980).

Beside the EDM technique *apatites* with low track densities were also analysed using the population method (GLEADOW, 1981). For the population method spontaneous and induced tracks were revealed and counted in separate sample aliquots. Spontaneous tracks in the reactor aliquot were totally annealed prior to irradiation by heating at 500 °C for 6 h. After irradiation spontaneous and induced fractions were similarly mounted on glass in epoxy, polished to reveal internal surfaces and simultaneously etched in 5 N HNO$_3$ at 20 °C for 20 sec. For each sample, track densities were determined on prismatic faces. *Lengths* of confined spontaneous tracks in apatite were measured with a Zeiss Morphomat 30 semi-automatical image analysis system.

Thermal irradiations were carried out in the J1 facility of the HERALD reactor, Aldermaston, UK, and in the thermal neutron facilities of the PLUTO and DIDO reactors, Harwell, UK. Neutron fluences were monitored by counting induced tracks in etched muscovite detectors against two uranium dosimeter glasses SRM-612, CN-1 and CN-2 (HURFORD and GREEN, 1983). Ft ages of apatites and zircons were calculated using the ζ calibration approach (FLEISCHER and HART, 1972; HURFORD and GREEN, 1982). Values of ζ for zircon and apatite have been determined for each of these three dosimeter glasses (Tab. 1). Errors were calculated from Poissonian statistics together with an uncertainty on the ζ calibration factor. As a control of calibration and technique, mounts of the Fish Canyon tuff apatite and zircon and of zircon from the Buluk Member tuff were included in most of the irradiations. Comparison of ζ's measured by different workers on the same material reveals a spread of 20–25 per cent resulting from the use of different microscope conditions, personal counting bias, irradiation conditions, etc. (HURFORD, 1986a). For these reasons, we specify in table 1 the ζ's determined by each worker and used to determine the ages presented in this study. EDM analyses were subjected to the χ^2 test to detect whether the results contained any extra Poissonian scatter. Where the analyses failed the χ^2 test, the age was calculated by the mean individual crystal ρ_s/ρ_i ratio, which gives approximately the same age but makes allowance for the wider spread of individual crystal values (GALBRAITH, 1981).

For the *K–Ar age analyses* high purity concentrates of white mica and biotites were made from 15–30 kg samples using conventional crushing, shaking table and magnetic techniques. Potassium was determined using an IL flame photometer (PURDY and JÄGER, 1976). For the argon analyses 0.1 to 0.2 g aliquots of mineral were fused using a HF generator and the envolved gases were purified and on line measured as described previously (FLISCH, 1982).
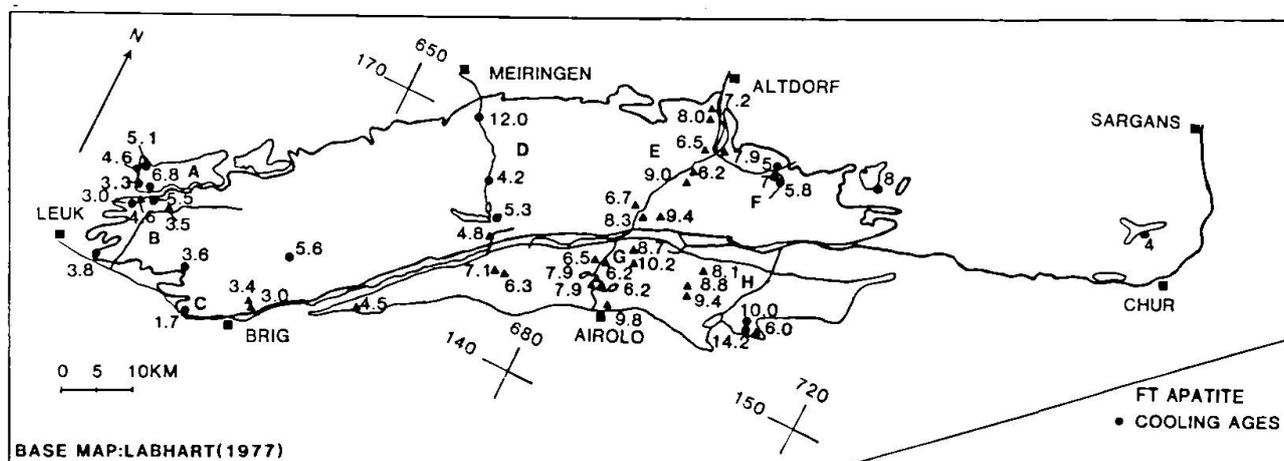

Fig. 3 The apatite fission track ages. The triangles are ages from WAGNER, REIMER and JÄGER (1977) and SCHAER et al. (1976). The capital letters represent the single regions which are discussed in the text. The coordinates are Swiss coordinates.
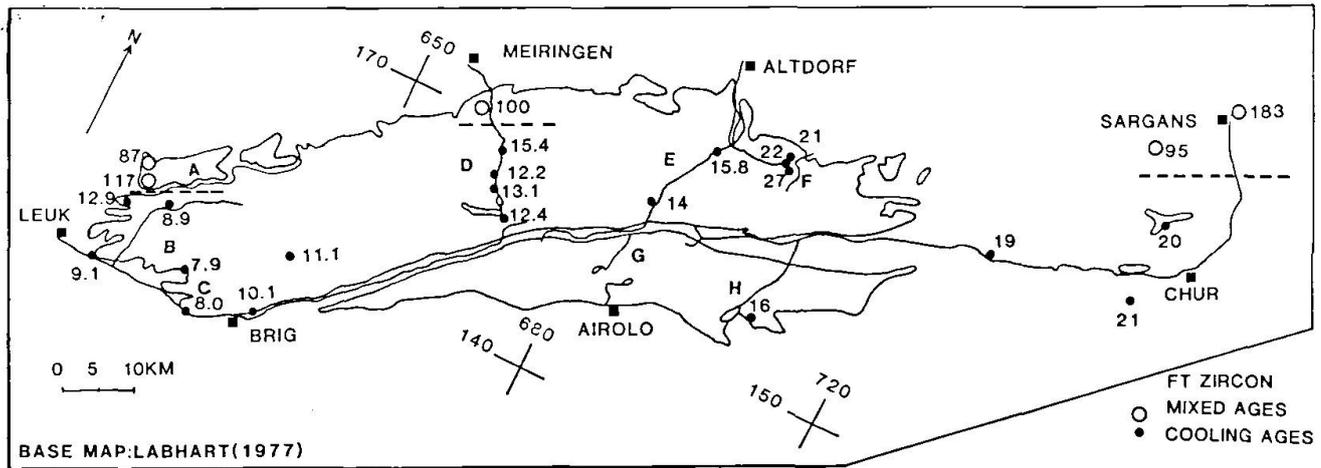
Fig. 4 The zircon fission track ages. The capital letters represent the single regions which are discussed in the text. The coordinates are Swiss coordinates.

5. Results

Ft apatite EDM and population ages and data on apatite standards are presented in table 1 (Fig. 3). Exact sample localities and brief descriptions of the samples are given in Appendix 1 with the exception of samples from Schaer et al. (1975) and Wagner et al. (1977). For apatite population analyse a minimum of 200 crystals were counted for each of the spontaneous and induced measurements. The paucity of spontaneous tracks in most samples which results from both low uranium content and low age as well as many fluid inclusions is reflected in the high errors on the calculated ages. The ft apatite ages show a regional variation and increase with altitude. From the slope of the line of the age vs. altitude diagrams it is possible to calculate the palaeo-uplift rates for the time span which is given by the highest and youngest age of the respective region. A distinct altitude dependence was found for 8 regions: Gastern-(A), north-western Aar-(B), south-western Aar-(C), Grimsel-(D), Reuss-(E), north-eastern Aar-(F), central Gotthard-(G) (Figs 5, 6, 7 and 8). The gradient of the ft apatite age plotted against sample elevation is taken to be the palaeo-uplift rate over the period given by the ft apatite ages (Figs 5, 6, 7 and 8). 4 samples of the northern part of the Grimsel-(D) and Reuss-(E) profile lie outside the age vs. elevation curves. Some of curves were supplied with former data fom Wagner et al. (1977) and Schaer et al. (1975). Although these authors used a different ft calibration method the similarity of these ages with our data indicates comparability within error limits of the ft apatite ages (Tab. 3).

Ft zircon sample ages and results on standards with zircon standards are presented in table 1. Exact sample localities and brief descriptions of the

samples are given in Appendix 1. The high track density in most samples which results from a high uranium content and the zonation of the uranium concentration as well as the dependence of its chemistry is reflected in the high errors on some zircon ages. Figure 4 shows the regional distribution of the zircon ages (Tab. 1). The ages in the massifs increase from west to east but a few samples at the northern edge of the Aar massif and the region north of the Vättis window near Chur are significantly older (Fig. 4). In contrary to the apatite ages the ft zircon ages do not increase with the altitude as is shown in figure 10.

The results of the *confined lengths* measurements of the samples KAW 2617, KAW 2702, KAW 2782 and KAW 2207 give mean lengths of 13.5–14.5 μm with 1 σ errors of ± 0.05 μm (Wagner, 1985). Because of the paucity of confined tracks in KAW 2617, KAW 2702 and KAW 2782 it was not possible to measure more than 50 tracks in these samples. In the sample KAW 2207, where 100 confined tracks were measured, the mean length was 14.50 μm and the standard deviation 1.31. The lengths measurements of 13.5–14.5 μm correspond to undisturbed steady cooling behaviour which is confirmed by the result of KAW 2207 the oldest apatite ft age sample within this study (Gleadow et al., 1983).

Table 2 details the analytical data of *K–Ar analyses* on biotite and white mica samples. Exact sample localities and brief descriptions of the samples are given in Appendix 1. All errors are 1 sigma and typically ± 1.5% except of the chlorite rich sample KAW 2264. A compilation of all samples and their localities is presented in figure 1. The K–Ar ages increase from north to south (Tab. 2 and Fig. 1); the biotite ages in the north are around 200 Ma while the ages in the south only give results around 20 Ma. An exception is the white mica age

Tab. 1 Fission track analytical data for Aar- and Gotthard massif samples and Fish Canyon standards. (Note: track densities (ρ) are as measured as ($\times$ 10^5 tracks cm^{-2}); N is the total amount of counted tracks; P(χ^2) is probability of obtaining χ^2 value for v degrees of freedom where v = no. crystals - 1; mean ρ_s/ρ_i ratio used to calculate age and uncertainty where P(χ^2) < 5%; for population method analyses, relative standard error of mean track count (s´) is shown.)

Sample Locality Elevation	Mineral and No. crystals	Spontaneous ρ_s	(N_s)	Induced ρ_i	(N_i)	Pχ^2% or s´%	ρ_s/ρ_i ±1σ	Irrad. No.	Glass	Dosimeter ρ_d	(N_d)	Age Ma ±1σ
KAW 2 Tödi 2000m	apatite1 4	1.54	8	23.7	123	49	0.065 ±0.024	BeH11	612	8.9	(4871)	8.9±3.2
KAW 65 Tenmatte 1460m	zircon2 10	19.87	485	34.13	833	15	0.582 ±0.033	Be44	CN-1	2.414	(4422)	8.9±0.8
KAW 128 Electra 900m	zircon1 10	1.56	171	5.28	578	28	0.29 ±0.026	BeH15	CN-1	9.14	(4461)	15.8±1.5
KAW360 Electra 900m	zircon2 10	23.8	464	39.8	777	87	0.597 ±0.035	Be45	CN-1	2.517	(2845)	10.1±0.9
KAW 578 Val Cristallina 1910m	apatite1 8	1.6	29	19.9	341	5	0.085 ±0.016	BeH6	612	7.73	(5744)	10.1±2.1
KAW 2207 Guttannen 720m	apatite3 20	4.754	253	2.272	1209	pass	2.09 ±0.027	Be28	612	3.372	(4000)	12.0±0.9
	zircon3 10	11.23	1628	2.148	310	pass	5.22 ±0.032	Be29	612	1.134	(2448)	100±7
KAW 2208 Handegg 1350m	zircon3 20	3.192	356	5.168	1386	pass	0.617 ±0.028	Be32	CN-1	3.505	(4000)	12.2±0.6
KAW 2213 Grimselpass 2160m	apatite1 12	5.35	31	53.05	307	80	0.101 ±0.019	Be28	612	3.412	(1241)	5.3±1.1
	zircon3 12	5.125	855	7.75	1327	pass	0.66	Be29	612	1.109	(2448)	12.4±0.6
KAW 2219 Chuenzen tennlen 1586m	apatite1 14	5.3	19	66.6	236	26	0.081 ±0.019	Be28	612	3.3	(1241)	4.2±1.1
	zircon3 10	5.037	907	7.148	1287	pass	0.704 ±0.031	Be29	612	1.094	(2448)	13.1±0.7
KAW 2408 Tschingel brücke 1200m	zircon1 4	15.3	91	53.1	316	100	0.288 ±0.034	BeH15	CN-1	9.18	(4461)	15.5±2.0
KAW 2518 Göschenen 1500m	zircon1 10	30.41	365	84.08	1009	34	0.362 ±0.022	BeH10	CN-1	5.85	(5271)	13.5±1.0
KAW 2608 Schwarze Hörner 2400m	apatite1 10	0.7	18	13.2	320	<2	-	BeH6	612	7.43	(5744)	6.4±1.7
	zircon1 3	138.0	361	55.0	144	15	2.507 ±0.247	BeH10	CN-1	6.02	(5271)	96.0±10
KAW 2609 Sargans 540m	zircon1 12	103.0	653	23.0	145	<2	-	BeH10	CN-1	5.9	(5271)	168±16
KAW 2612 Rothenbrunnen 630m	zircon1 8	26.72	400	45.55	682	<2	0.558 ±0.073	BeH10	CN-1	5.97	(5271)	21.3±2.8
KAW 2616 Staldi 1440m	apatite2 200/200	0.611	138	17.74	1780	4	-	Be41	612	4.125	(2889)	5.1±0.6
	zircon2 11	124.0	924	21.9	163	99	5.669 ±0.482	Be44	CN-1	2.429	(4422)	86.9±9.3

KAW 2617 Nieder- gampel 660m	apatite2 200/200 zircon2 10	0.775 13.7	175 251	31.24 24.1	7053 443	3 97	- 0.567 ±0.045	Be41 Be45	612 CN-1	4.244 2.392	(2889) (2845)	3.8±0.4 9.1±0.9
KAW 2662 Lötschberg 1220m	apatite2 12	0.904	65	36.85	2649	91	0.025 0.003	BeH12	612	10.42	(7632)	4.6±0.6
KAW 2663 Lötschberg 1220m	apatite2 12	0.555	29	31.28	1635	99	0.018 ±0.003	BeH11	612	10.4	(7632)	3.3±0.6
KAW 2664 Lötschberg 1220m	zircon2 12	24.3	434	29.1	520	29	0.835 ±0.054	Be44	CN-1	2.434	(4422)	12.9±1.2
KAW 2702 Hockenhorn 3020m	apatite2 200/200 zircon2 13	0.306 160.3	69 1421	6.754 21.1	1525 187	3 96	- 7.599 ±0.5991	Be42 Be44	612 CN-1	4.142 2.439	(2737) (4422)	6.8±0.8 117±12
KAW 2703 Hockenhorn 3293m	apatite2 12	0.103	76	34.7	2560	60	0.030	Be12	612	10.38	(7632)	5.5±0.7
KAW 2761 Eggishorn 2870m	apatite2 200/200 zircon2 10	0.563 29.1	127 423	14.77 38.6	3334 560	3 75	- 0.755 ±1.1	Be42 Be44	612 CN-1	4.108 2.444	(2737) (4422)	5.6±0.6 11.7±1.1
KAW 2780 Wiwannihorn 2540m	apatite2 12 zircon2 10	1.014 18.3	44 235	52.73 35.1	2289 451	31 99	0.019 0.521 ±0.042	BeH12 Be45	612 CN1	10.26 2.253	(7632) (2845)	3.6±0.6 7.9±0.8
KAW2782 Baltschieder 650m	apatite2 200/200 zircon2 10	0.176 32.9	141 249	15.35 63.7	3467 483	3 50	- 0.516 ±0.04	Be42 Be44	612 CN1	4.142 2.45	(2737) (4422)	1.7±0.2 8.0±0.8
KAW2983 Ilanz 700m	zircon1 9	20.73	569	43.5	1194	<2	-	BeH10	CN1	6.00	(5271)	19.2±1.7
KAW3120 Fruttstock 2800m	apatite1 10 zircon1 10	0.77 23.44	28 156	10.3 56.6	412 377	<2 10	- 0.414 ±0.039	BeH6 BeH15	612 CN1	7.40 9.25	(5744) (4461)	7.7±1.7 22.4±2.3
KAW3121 Brunnibach 2240m	apatite1 15 zircon1 12	14.5 41.1	53 303	32.12 79.55	1168 586	22 10	0.045 ±0.006 0.517 ±0.037	BeH11 BeH15	612 CN1	8.49 9.19	(4871) (4461)	5.9±0.9 27.8±2.3
KAW3123 Maderanertal 1480m	apatite1 14 zircon1 10	17.1 19.8	58 248	413.4 51.4	1400 642	43 <2	0.041 ±0.006 0.4	BeH11 BeH15	612 CN1	8.01 9.12	(4871) (4461)	5.1±0.7 21.6±2.4
KAW3200 Scopi	apatite1 14	25	52	220.2	458	74	0.114	BeH11	612	8.17	(4871)	14.2±2.4
KAW3215 Vättis 1060m	apatite1 10 zircon1	0.58 1.0	14 29	15.7 24.4	374 82	7 69.0	0.037 ±0.01 0.354 ±0.079	BeH11 BeH15	612 CN1	7.81 9.24	(4871) (4461)	4.5±1.2 19.1±4.2
FCT3 Fish Canyon	apatite1 16	2.19	223	9.20	935	54	0.239 ±0.018	BeH6	612	7.55	(5744)	27.5±2.3
FCT3 Fish Canyon	apatite2 12	2.289	175	14.84	1134	99	0.154 ±0.013	BeH12	612	10.323	(7632)	28.6±2.8
FTBM4 Buluk	zircon2 10	9.432	447	9.010	427	73	1.047 ±0.071	Be44	CN1	2.438	4422	16.4±1.5

Note:

all ages with index 1 calculated with ζ SRM612 = 306 and ζ CN1 = 128
all ages with index 2 calculated with ζ SRM612 = 360 and ζ CN1 = 127
all ages with index 3 calculated for apatie ages with ζ SRM612 = 323 and
for zircon ages with ζ 612=337.5 and ζ CN1 = 112.8

Tab. 2   K–Ar analytical data for Aar- and Gotthard massif samples.

sample and locality	mineral and fraction	K (weight%)	$^{40}Ar_{rad}(x10^{-6})$ $cm^3(STP)/g$	$^{40}Ar_{rad}$ (%)	Age(Ma) $\pm1\sigma$
KAW65 Tenmatte	biotite 35-80	7.74	56.11	98.4	177.5 ±1.9
KAW89 Gastere	biotite 35-80	6.41	78.38	99.0	290.0 ±3.0
KAW2664 Lötschberg	biotite/chlorite 40-80	1.68	2.7	81.1	40.9 ±1.4
KAW2780 Wiwanni	biotite 40-100	6.47	10.27	96.1	40.1 ±0.5
KAW2782 Baltschieder	biotite 80-100	7.59	7.4	91.7	24.9 ±0.3
KAW3200 Scopi	biotite 35-80	7.6	51.17	68.8	17.2 ±0.3
KAW3215 Vättis	muscovite	8.9	113	97.6	300 ±2.9

of the Vättis window north of the Aar massif near Chur which gives an age of about 300 Ma.

6. Discussion and interpretation

6.1. THE FT APATITE AGE

The regional variations in the ft ages reveal the regional uplift pattern. Any one age directly gives the time which elapsed between passing the 120 °C isotherm and reaching the surface. Thus, an aver-

age cooling rate and an average uplift rate (if the geothermal gradient is known) can be calculated individually for each sample for cooling under 120 °C. According to WAGNER, REIMER and JÄGER (1977) the present morphology of the Alps is replaced by a peneplain surface at an altitude of 2200 m and a mean annual surface temperature of ~ 0 °C to calculate the cooling rates below 120 °C. By comparing a sample apatite age and elevation to this datum line, palaeo-uplift may be calculated up to the present day. For ft apatite cooling ages three cases are possible: A continous steady uplift would

Tab. 3   Comparision of ft ages.

Sample and locality	Age Wagner et al.(1977) Ma±1sigma	Age this work Ma±1sigma	difference Ma	difference of mean in %
159 Gondo	2.6±0.3	2.4±0.6	-0.2	-7.7
160 Kaserne	2.5±0.3	2.9±0.6	+0.4	+16.0
357 Serra	3.2±0.3	3.4±0.9	+0.2	+6.3
578 Cristallina	8.9±0.9	10.1±2.1	+1.2	+12

be revealed in an age vs. elevation diagram by a straight line intersecting the elevation axis at a depth of –1800 m. Increase or decrease of the uplift rates could be discerned in the age vs. elevation diagram from the intersection of the lines with different elevations on the y-axis, the rate given by the slope can be compared to the actual uplift rates. The following interpretations were made for the measured data, using a geothermal gradient of 30 °C/km and under the assumption of the peneplain surface model.

The calculated uplift rates for single regions of the Aar and Gotthard massifs can be deduced from figures 5, 6, 7 and 8. In general, an uplift of 0.5 mm/a occurred in the Grimsel (profile D) and Reuss valley (profile E) cross-section and in the eastern part of the Aar massif during the period of about 5 to at least 10 Ma. In contrast, a significantly faster uplift of 0.8–1 mm/a occurred in the west

from about 2 to at least 7 Ma. The palaeo-uplift rate in the Gotthard massif increased from east to west by about 0.3 mm/a to 0.5 mm/a between 5 to at least 14 Ma.

The connection between the constructed ft apatite zero age at –1800 m with the end of our uplift lines from the surface samples is shown in figures 5, 6, 7 and 8. The uplift rates of the Gastern region (A), the northwest of the Aar massif region (B) and the southwestern regions of the Aar massif (C) for the last 5 Ma have been calculated in this way. The palaeo-uplift rates for the Gastern region and for the north western Aar massif remain roughly the same for the last 7 Ma and correspond to the recent uplift rates of 0.8 mm/a which are determined by precision levelling geodetic measurements (WIGET and GUBLER, 1988). The uplift in the southwestern part of the Aar massif must have been accelerated in order to derive an apatite zero
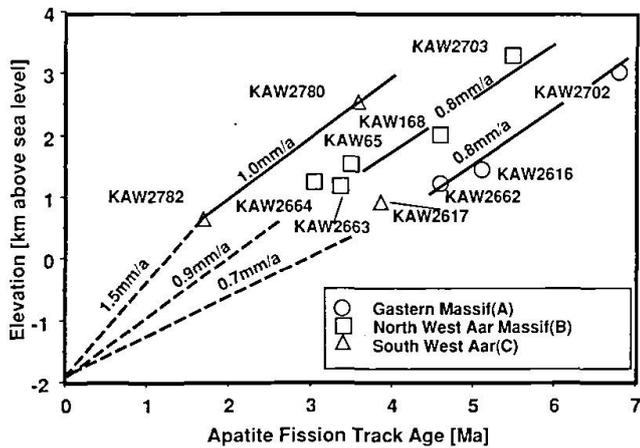

Fig. 5 Apatite ft age vs. elevation curves from the western part of the Aar massif. The 1 σ errors which are about 10% are given in table 1. KAW 65 and KAW 168 were taken from WAGNER et al. (1977).
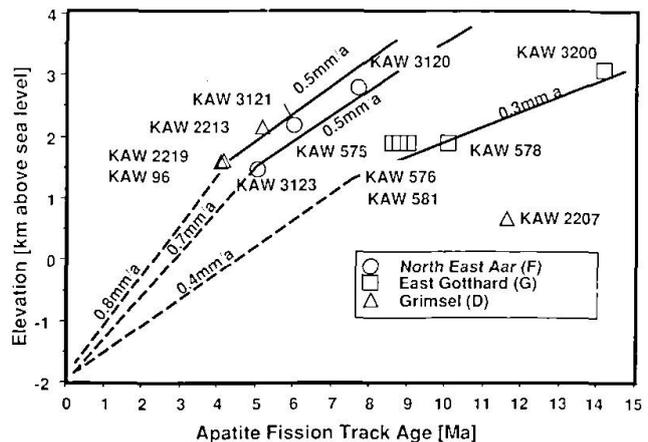

Fig. 6 Apatite age vs. elevation curves from the northeast Aar-, the eastern Gotthard- and the Grimsel region. The 1 σ errors which are about 10% are given in table 1. KAW 96, KAW 575, KAW 576 and KAW 581 were taken from WAGNER et al. (1977).
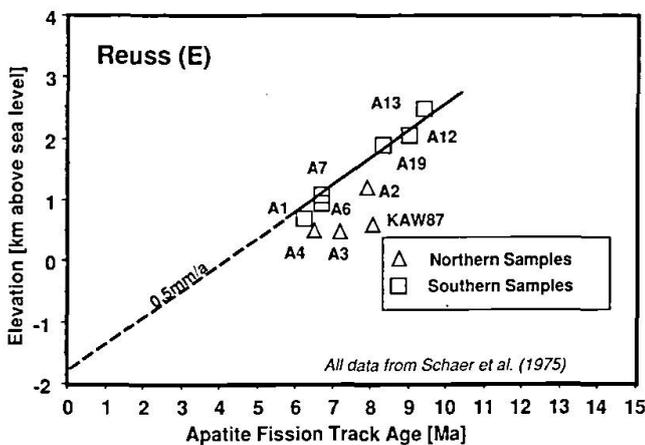

Fig. 7 Age vs. elevation curve of the Reuss region calculated from SCHAER et al. (1976). The northern sample points of the profile do not fit the curve. The 1 σ errors which are about 10% are given in table 1.
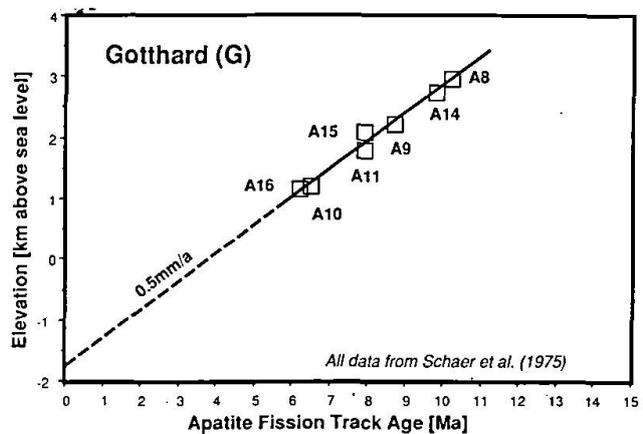

Fig. 8 Age vs. elevation curve of the Gotthard region calculated from SCHAER et al. (1976). The 1 σ errors which are about 10% are given in table 1.
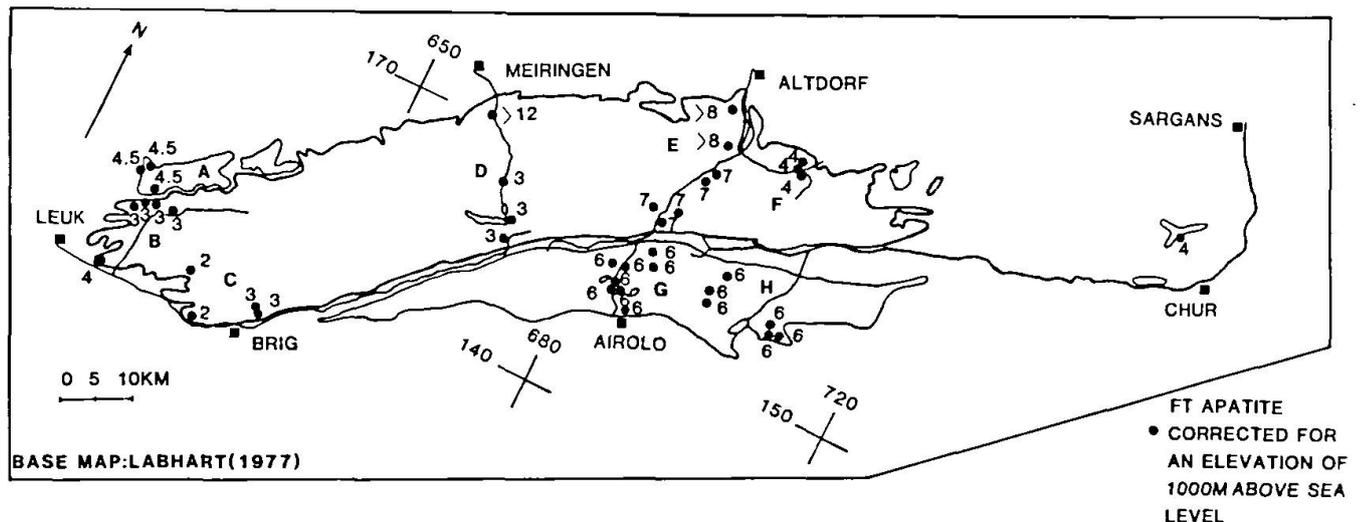
Fig. 9 The corrected apatite ft ages to a mean elevation of 1000 m above sea level.

age at a depth of –1800 m. The onset of the acceleration of the uplift rate can be derived as about 2–3 Ma from the intersection of the 1 mm/a line of uplift with the 1.5 mm/a line (Fig. 5). This 2–3 Ma demonstrates the approximate beginning of uplift of the Brig area which corresponds with the beginning of the current Chur uplift at about 3 Ma (FLISCH, 1986). The uplift rate of 1.5 mm/a determined from the age vs. altitude diagram and the apatite zero ages corresponds well to the current uplift rate determined by WIGET and GUBLER (1988).

The palaeo-uplift rate for the Grimsel profile (D) is 0.5 mm/a from 4 to at least 6 Ma. In order to reach the apatite zero age at a depth of –1800 the uplift rate had to be accelerated to a mean of 0.8 mm/a sometime during the last 4 Ma (Fig. 6). This uplift rate is also comparable to the recent uplift rate determined by WIGET and GUBLER (1988). The sample KAW 2207 (12 Ma, Guttannen) lies significantly below this rate. (In this case the possibility of a mixed age could be excluded by confined length measurement.) Since a sequence of small displacements is found in this region (pers. communication T. LABHART) these age differences imply a different uplift regime in the northern part of the Grimsel profile (D).

The palaeo-uplift in the southern part of the Reuss valley has remained constant at 0.5 mm/a for the last 10 Ma (Fig. 7). The current uplift rates in this region are 0.6–0.7 mm/a and are thus somewhat higher, but within the same margins of error (WIGET and GUBLER, 1988). Ft ages of the southern Reuss profile show in the age vs. elevation curve no N–S trend since they are governed by real uplift (Fig. 7). As in the Grimsel profile the northern samples of the Reuss profile (E) KAW 87, A2, A3 and A4 lie significantly outside the age vs. elevation curve. It is probable that the age differences here

also result from a different uplift regime along several fault zones.

Further to the east in the north-east Aarmassif region (F) the uplift rate during the period of 5 to 8 Ma is 0.5 mm/a, whereas the uplift has increased sometime during the last 5 Ma to a mean of 0.7 mm/a (Fig. 6). There are no recent geodetic measurements for this region.

In the central Gotthard profile the uplift remained constant for the last 10 Ma (Fig. 8). In this region current uplift rates of 1.0 mm/a have been measured (WIGET and GUBLER, 1988). In the eastern Gotthard the palaeo-uplift rates of our profile increased from 0.3 mm/a to 0.4 mm/a. In contrast the current uplift rates at with 0.8 mm/a are higher. This discrepancy in these regions between our data and the current uplift rates imply that the onset of the fast uplift behaviour in central and east Gotthard region must be very young.

Although the uplift rates suggest a fairly equal uplift pattern throughout the Aar massif in the time between 5 to 10 Ma different regions have been cooled below the 120 °C isotherm at different times, as can be seen in figure 9. In the whole of the Aar massif the apatite age decreases from N to S. The northern edge has therefore uplifted earlier than the southern edge of the massif. Also along the W–E axis of the massif the uplift of individual regions under 120 °C has occurred at different times. The central and eastern part of the Gotthard massif cooled below 120 °C at the same time despite different uplift rates. GUBLER et al. (1981) describe a linear increase of the current uplift rates from Andermatt (southern part of the Reuss valley) with an uplift minimum in this region compared to both the west and the east. The current uplift maxima can be observed in the west near Brig and in the east near Chur. The corrected apatite ages of the Aar massif show the same tendency,

since the ages of the Reusstal decrease to the west as well as to the east. The decrease of the corrected ft ages to the current uplift maxima corresponds to the increase of the uplift rates as determined by the apatite zero age, and thereby approaches recent uplift maxima.

6.2. THE FT ZIRCON AGES

At the north edge of the Aar massif and north to Vättis the ft zircon ages vary quite widely between 87 and 183 Ma. They cannot be attached to any geological event. The ages occur within the very low grade metamorphism where mixed ages between Variscan and Alpine cooling are to be expected. Because of these reasons we divided the zircon ages into two zones: a northern zone with mixed age values and a southern zone with cooling ages (Fig. 4).

The northernmost cooling ages occur in the north-east Aarmassif region (profile F, Figs 2 and 4). The reason for interpreting these ages as cooling ages is the fact that Gnos (1988) found the Stilpnomelane-out isograd between the southern sample KAW 3121 (27 Ma) and the two northern samples KAW 3120 (22 Ma) and KAW 3123 (22 Ma) (Figs 1 and 2). These ages overlap within the 2 sigma error. The large error arises probably from the different chemistry of the samples and from the variation in the metamict conditions of the zircons.

Thus the ft zircon mixed age zone occurs to the east of the Aar massif, between Sargans and Chur, namely within the Stilpnomelane zone (FREY, 1987). The westerly continuation of the ft zircon mixed age zone runs through the Aar massif itself. In the Grimsel cross-section (profile D, Figs 2 and 4) the boundary between mixed ages/cooling ages may be drawn between sample KAW 2207 (100 Ma, Guttannen) in the north and KAW 2408 (15.4 Ma, Tschingelbrücke) further to the south (Figs 1 and 4). To the west this boundary may be continued into the southern part of the Gasternmassif (profile A, Figs 2 and 4).

The upper temperature limit of the boundary between the ft zircon mixed age zone to the cooling age zone can be derived from several independent investigations in this region. Since the boundary of the zircon mixed age to the cooling age zone occurs north of the beginning of rejuvenation in the Rb–Sr biotite (300 ± 50 °C) and K–Ar biotite (300 ± 50 °C) systems (WÜTHRICH, 1965; JÄGER et al., 1967; PURDY and JÄGER, 1976) the resetting of an ft zircon age has to occur under the closure temperature of these systems. In the north-western edge of the Aar massif also very close to the boundary mixed ages/ zircon cooling ages several temperature estima-
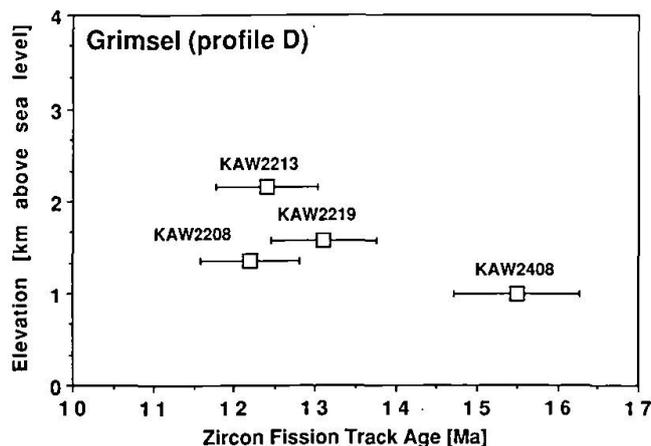

Fig. 10   Age vs. elevation scatter of zircon ft ages from the Grimsel profile.

tions exist. MULLIS (1979) has estimated metamorphic PT-conditions in the low grade Doldenhorn area of at least 260 °C. Quartz recrystallization (275–290 °C) in the Grimsel profile (profile D) starts north of KAW 128 (VOLL, 1976) which belongs to the cooling age zone. It follows that the temperature range of the zircon mixed age zone (partial annealing zone) lies between 200 to at least 250 °C (the shortening of tracks in zircons start at a temperature of about 200 °C, see introduction) but below 300 °C. In the area described above the rocks were situated in a shallow crustal level (< 200 °C) during the Mesozoic. Tertiary tectonics lead to a detachment and crustal thickening after Eocene/ lower Oligocene (ca. 40 Ma; end of Helvetic flysch sedimentation) (HERB, 1965). Since uplift and erosion of the Helvetic sediments began in Tortonian time (ca. 10 Ma ago) the time span for metamorphic heating to temperatures between 200 to 250 °C was about 30 Ma.

Our zircon cooling age results show the earliest cooling in the east to below 200 to 250 °C (closure temperature, see introduction) at about 21–27 Ma (during lower Miocene) in the northeast Aarmassif region (Fig. 4, profile F), followed by a later cooling in the west at about 10 Ma (during upper Miocene). For a geothermal gradient of 30 °C/km the cooling below 200 to 250 °C can be assumed at a depth of 6–8 km 23 Ma ago for the northeast Aar massif region (profile F) and for the samples of the Brig region, also at a depth of 6–8 km, 10 Ma ago. The zircon cooling ages of the Aar massif demonstrate a cooling sequence for the massifs from east to the west. This cooling sequence results in an updoming which starts in the complete massif from east to west and from north to south. As mentioned above our ft zircon cooling ages do not increase with the altitude (Fig. 10) probably because of the N–S trend of the ages.

6.3. THE K–Ar AGES

As Jäger et al. (1967) and Purdy and Jäger (1977) pointed out three different types of K–Ar mica ages occur in the Aar and Gotthard massifs: From north to south a zone of pre-alpine ages, a transition zone from pre-Alpine to Alpine ages and a zone of Alpine ages. Our K–Ar data fit well into these zones and supplement earlier results (Tab. 3). Within the massifs, KAW 89 gave a pre-alpine age, KAW 2664, 2780 and 2782 are typical ages for the transition zone and KAW 3200 was considered as Alpine cooling age (Tab. 2 and Fig. 1). KAW 65 and KAW 89 belong to the temperature range < 300 ± 50 °C, KAW 2664, 2780 and 2782 to the temperature range of 300 ± °C and the southern sample KAW 3200 to the temperature range > 300 °C. Since a white mica concentrate of KAW 3215 from the Vättis window was dated as pre-Alpine it follows that temperatures were not much higher than 350 ± 50 °C because the muscovite age is not reset.

6.4. COMPARISION OF DIFFERENT AGES

In principle, the different cooling ages measured on coexisting minerals should allow us to construct the cooling history of a rock from 500 °C to the present temperature. However, in practice there are often limitations presented by the paucity of either white mica, biotite, zircon or apatite, low maximum temperatures, etc. In this work the ft zircon and apatite ages are well-suited for such comparison because they were determinated on about 20 rocks (Tab. 1). The difference between the ages of these minerals including the biotite ages gives the time span during cooling from 300 to 120 °C and is a direct measure of the cooling rate within this temperature interval. The representative cooling curves for each

region is shown in figures 11, 12 and 13. Some of the curves have been completed by the addition of K–Ar biotite and Rb–Sr biotite data points from Purdy and Jäger (1976) and Dempster (1986). The smallest age differences (14 Ma to 10 Ma to 3.4 Ma) are found in the Brig region (Fig. 13). The northeast Aarmassif region and the region of Vättis near Chur give the largest age differences (22 Ma to 5 Ma for the northeast Aarmassif region and 19 Ma to 4.5 Ma for Vättis) (Fig. 11).

Comparision of the different temperature intervals 300–240 °C and 240–120 °C show that cooling is not identical for the two temperature intervals. This indicates temporal and regional changes of cooling and uplift in the Aar massif. The Chur region and the northeast Aarmassif region show both a very slow cooling (7 °C/Ma) in the time span between 22 and 4 Ma and an acceleration of cooling during the last 4 Ma (see 6.1., Fig. 11). The overall cooling rate of the Grimsel profile is about 15 °C, quite constant in the time between 27 and 4 Ma, but at some time during the last 4 Ma, an acceleration took place (see 6.1. and Fig. 12). The Rb–Sr muscovite age of 27 Ma was interpreted as a formation age at a temperature of 450 °C (Dempster, 1986). The cooling of the Reuss profile is constant during the last 14 Ma (Fig. 11). In the region of Brig the acceleration of cooling started even in the temperature range under 300 °C between 14 and 3 Ma and is continuing up to the present (see 6.1. and Fig. 13). Therefore the cooling under 300 °C started ealier and slower in the eastern part of the Aar massif and continued later but faster in the western part of the massif.

7. Conclusions

Fission track age determinations on zircons and apatites on a series of samples from the Helvetic
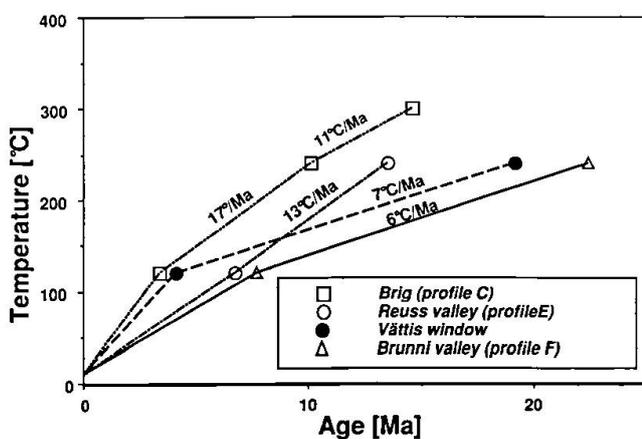

Fig. 11 Cooling curve from the Brig region based on the different blocking temperatures. K–Ar biotite age from Purdy and Jäger (1976).
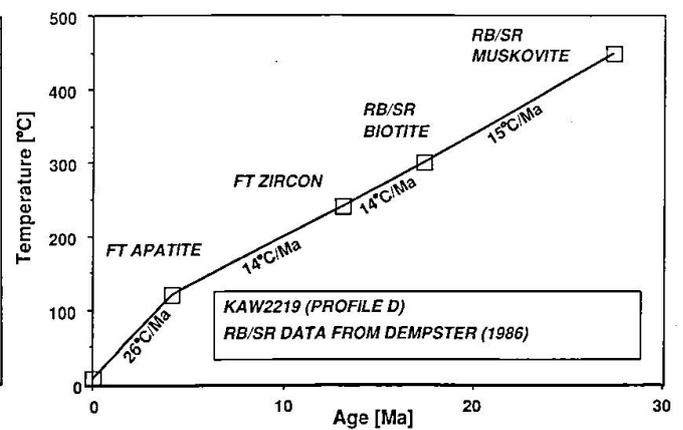

Fig. 12 Cooling curves from different regions of the Aar massif based on the different blocking temperatures.
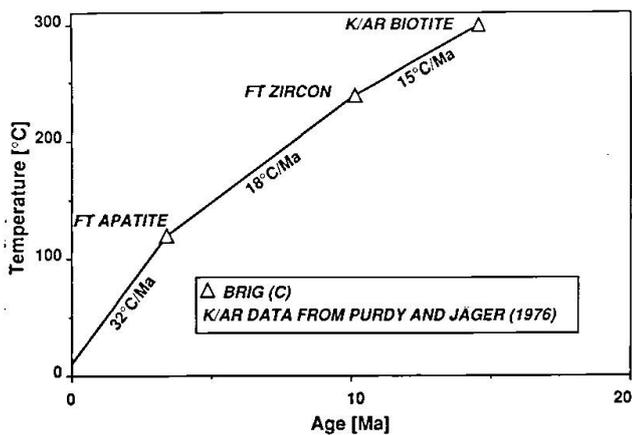
Fig. 13 One complete cooling curve from the Grimsel region based on the different blocking temperatures. Rb–Sr data from DEMPSTER (1986).

zone of the Central Swiss Alps provide new information about the uplift patterns of the Aar and Gotthard massifs:

(a) Comparision of the ages allow the reconstruction of the cooling rates during the last 27 Ma. Cooling took place in the eastern part of the massif earlier (Lower Miocene) than in the western part of the massif (Upper Miocene).

(b) The zircon cooling ages of the Aar massif demonstrate a cooling sequence for the massifs in the time 27 to 8 Ma from east to west and from north to south. This cooling sequence results in an earlier updoming in the east in Lower Miocene followed by later updoming in the west in Upper Miocene.

(c) The 200° to at least 250 °C ft zircon mixed age zone can be followed up throughout the northern Aar massif and its eastern continuation to the north of the Vättis window.

(d) ft apatite ages published previously for Alpine samples can be compared to ft apatite ages published today even when different calibration methods were used.

(e) In both massifs this updoming can also be shown from the increasing palaeo-uplift rates from west to east from 0.3 to 1.0 mm/a (Figs 4, 5, 6 and 7).

(f) Sometime during the last 2–3 Ma the influence of the uplift maxima from the Visp and Chur were worked out. The Reuss valley forms the axis between the Visp and Chur region with a minimum uplift rate of 0.5 mm/a continuing into the present.

(g) In the northern part of the Aar massif faulting is more probable than tilting (Figs 6 and 7).

(h) Under the assumption of a gradient of 30 °C/km cooling rates agree well with the uplift rates which is a good hint for an undisturbed uplift regime.

(i) The Gotthard massif was uplifted in the western part with 0.5 mm/a faster than in the eastern part with 0.3 mm/a during Upper Miocene.

(k) K–Ar ages fit well into the previously established age pattern of JÄGER et al., 1967 and PURDY and JÄGER, 1977.

References

BHANDARI, N., BHAT, S.G., LAL, D., RAJAGOPALAN, A.S., TAMHANE, A.S. and VENKATAVARADAN, V.S. (1971): Fission Fragment Tracks in Apatite: Recordable Track Lengths. Earth. Planet. Sci. Letts. 13, 191–199.

BOYER, W.S. and ELLIOTT, D. (1982): Thrust Systems. Bull. amer. Assoc. Petroleum Geol. 66/9, 1196–1230.

DODSON, M.H. (1973): Closure temperature in cooling geochronological and petrological systems. Contributions to Mineralogy and Petrology 40, 259–274.

DEMPSTER, T. (1986): Isotope systematics in minerals: biotite rejuvenation and exchange during Alpine metamorphism. Earth Planet. Sci. Letts. 78, 355–367.

FLEISCHER, R.L., PRICE, P.B. and WALKER, R.M. (1965): Ion explosion spike mechanism for formation of charged particle tracks in solids. J. Appl. Phys. 36, 3645–3652.

FLEISCHER, R.L. and HART, H.R. (1972): Fission track dating: techniques and problems. In: BISHOP, W.W., MILLER, J.A. and COLE, S. (eds) Calibration of Hominid Evolution. Scottish Academic Press, Edinburgh, 135–170.

FLISCH, M. (1982): Potassium argon analysis. In: ODIN, G.S. (ed.) Numerical dating in stratigraphy. John Wiley, Chichester, 151–158.

FLISCH, M. (1986): Die Hebungsgeschichte der ostalpinen Silvretta-Decke seit der mittleren Kreide. Bulletin der Vereinigung schweizerische Petroleum-Geologen und Ingenieure 53, 23–49.

FRANK, E. and STETTLER, A. (1979): K–Ar and ^{39}Ar–^{40}Ar systematics of white K-mica from an Alpine metamorphic profile in the Swiss Alps. Schweiz. Mineral. Petrogr. Mitt. 59, 375–394.

FREY, M. (1987): Low temperature metamorphism. Chapman and Hall, New York, pp. 351.

GALBRAITH, R.F. (1981): On statistical models for fission track counts. Math. Geol. 13, 471–488.

GLEADOW, A.J.W. (1981): Fission track dating methods: what are the real alternatives? Nucl. Tracks 5, 3–14.

GLEADOW, A.J.W. and BROOKS, C.K. (1979): Fission Track dating, thermal histories and tectonics of igneous intrusions in East Greenland. Contr. Mineral. Petrol. 71, 45–60.

GLEADOW, A.J.W. and DUDDY, I.R. (1981): A long-term track annealing experiment for apatite. Nucl. Tracks 5, 169–174.

GLEADOW, A.J.W and LOVERING, J.F. (1977): Geometry factor for external detectors in fission track dating. Nucl. Track Detection 1, 99–102.

GLEADOW, A.J.W., DUDDY, I.R., and LOVERING, J.F. (1983): Fission track analysis: a new tool for the evaluation of thermal histories and hydrocarbon potential. Austrl. Petrol. Explor. Assoc. J. 23, 93–102.

GLEADOW, A.J.W., HURFORD, A.J. and QUAIFE, D.R. (1976): Fission track dating of zircon – improved etching techniques. Earth Planet. Sci. Letts. 33, 273–276.

GNOS, E. (1988): Geologie und Petrographie des westlichen Brunnitals (Maderanertal, Kanton Uri) (unpubl. Diploma Thesis).

GUBLER, E., KAHLE, H.G., KLINGELE, E., MÜLLER, ST. and OLIVER, R. (1981): Recent crustal movements in Switzerland and their geophysical interpretation. Tectonophysics 71, 125–152.

HAMMERSCHMIDT, K. WAGNER, G.A. and WAGNER, M. (1984): Radiometric dating on research drill core Urach III: A contribution to its geothermal history. J. Geophys. Res. 54, 97–105.

HARRISON, T.M., ARMSTRONG, R.L., NAESER, C.W. and HARAKAL, J.E. (1979): Geochronology and thermal history of the Coast Plutonic complex, near Prince Rupert BC, Can. J. Earth Sci. 16: 400–410.

HERB, R. (1965): Das Tertiär der helvetischen Decken der Ostschweiz. VSP-Bull., 31, 81, 135–151.

HURFORD, A.J. (1986a): Application of the fission track method to young sediments: principles, methodology and examples. In: HURFORD, A.J., JÄGER. E. and TEN CATE, J.A.M. (eds) Dating young sediments, 393 pp.

HURFORD, A.J. (1986b): Cooling and uplift patterns in the Leopontine Alps South Central Switzerland and an age of vertical movement on the Insubric fault line. Contrib. Mineral. Petrol. 92, 413–427.

HURFORD, A.J. and GREEN, P.F. (1982): A users guide to fission track dating calibration. Earth Planet. Sci. Letts. 59, 343–354.

HURFORD, A.J. and GREEN, P.F. (1983): The Zeta age calibration of fission-track dating. Isotope Geoscience, 1, 285–317.

JÄGER, E. NIGGLI, E. and WENK, E. (1967): Rb-Sr-Altersbestimmungen an Glimmern der Zentralalpen. Beitr. geol. Karte Schw. 134, 1–67.

KRISNASWAMI, S., LAL, D., PRABHU, N. and MACDOUGLAS, D. (1974): Characteristics of fission tracks in zircon: applications to geochronology and cosmology. Earth Planet. Sci. Letts. 22, 51–59.

LAKATOS, ST. and MILLER, D.S. (1983): Fission-track analysis of apatite and zircon defines a burial depth of 4 to 7 km for lowermost Upper Devonian, Catskill Mountains, New York. Geology 11, 103–104.

LABHART, T.P. (1977): Aarmassiv und Gotthardmassiv. Sammlung. Geol. Führer 63, Borntraeger Berlin–Stuttgart, 173 pp.

MULLIS, J. (1979): The system methane-water as geologic thermometer and barometer from the external part of the Central Alps. Bull. Mineral. 102, 526–536.

NAESER, C.W. and FAUL, H. (1969): Fission Track Annealing in Apatite and Sphene. J. of Geophysical Research, 74, 2, 705–710.

NAESER, C.W., IZETT, G.A. and OBRADOVICH, J.D. (1980): Fission track and K–Ar ages of natural glasses. Bull. US. Geol. Surv. 1489, pp. 31.

NEUGEBAUER, H.J., BRÖTZ, R. and RYBACH, L. (1980): Recent uplift and the present stress field along the Swiss Geotraverse Basel–Chiasso. Eclogae geol. Helv. 73, 2, 489–512.

PFIFFNER, O.A., FREI, W., FINCKH, P. and VALASEK, P. (1988): Deep seismic reflection profiling in the Swiss Alps: Explosion seismology results for line NFP 20-East. Geology, 16, 11, 987–990.

PURDY, J.W. and JÄGER, E. (1976): K–Ar ages on rock-forming minerals from the Central Alps. Mem. Ist. Geol. Mineral. Univ. Padova, 30.

SCHAER, J.P., REIMER, G.M. and WAGNER, G.A. (1975): Actual and ancient uplift rate in the Gotthard region, Swiss Alps: a comparision between precise levelling and fission track apatite age. Tectonophysics 29, 293–300.

SCHALTEGGER, U. (1986): Mineralbildung in der Gneiszone von Erstfeld. Schweiz. Mineral. Petrogr. Mitt., 59, 3, 395–412.

STEIGER, R.H. and Jäger, E. (1977): Subcommission on geochronology: convention on the use of decay constants in geo- and cosmochronology. Earth. Planet. Sci. Lett. 24, 242–248.

TRÜMPY, R. (1980): Geology of Switzerland a guide book, Part A: An outline of the geology of Switzerland.

VOLL, G. (1976): Recrystallization of Quartz, Biotite, Feldspars from Erstfeld to the Leventina Nappe, Swiss Alps, and its Geological Significance. Schweiz. Mineral. Petrogr. Mitt., 56, 641–647.

WAGNER, G.A. (1968): Fission track dating of apatites. Earth. Planet. Sci. Lett. 4, 411–415.

WAGNER, G.A. and REIMER, G.M. (1972): Fission track tectonics: the tectonic interpretation of fission track apatite ages. Earth Planet. Sci. Letts. 4, 263–268.

WAGNER, G.A., REIMER, G.M. and JÄGER, E. (1977): Cooling ages derived by apatite fission track, mica Rb-Sr and K–Ar dating: the uplift and cooling history of the Central Alps. Mem. Ist. Geol. Mineral. Univ. Padua, 30.

WAGNER, M. (1985): Spaltspurendatierungen am Bohrkern Urach III – Ein Beitrag zur Wärmegeschichte der geothermischen Anomalie Urach. Diss. Univ. Heidelberg (unpubl.).

WIGET, A. and GUBLER, E. (1988): Beitrag der Geodäsie zur Geodynamik der Alpen. Bull. Ver. schweiz. Petroleum-Geol. u. Ing. 54, 9–14.

WÜTHRICH, H. (1965): Rb-Sr-Altersbestimmungen am alpin metamorph überprägten Aar-Massif. Schweiz. Mineral. Petrogr. Mitt., 45, 2, 875–971.

Appendix 1: list of samples

Sample	Locality	Swiss National Coordinate System	Rock Type
KAW 2	Tödi	715.620/186.500	granite
KAW 65	Tenmatte	627.850/140.150	biotite-gneiss
KAW 89	Gastere	622.000/144.200	biotite-Granite
KAW 128	Gurtnellen	691.225/176.550	granite
KAW 360	Electra-Massa	643.500/132.400	augen-gneiss
KAW 578	Val Cristallina	705.390/160.110	granodiorite
KAW 2207	Guttannen	661.500/170.900	biotite-granite gneiss
KAW 2208	Handegg	666.500/160.300	biotite-granite
KAW 2213	Grimselpass	669.000/157.500	biotite-granite gneiss
KAW 2219	Chuennzen-tennlen	667.600/161.300	biotite-granite
KAW 2408	Tschingelbrücke	666.200/166.180	granite
KAW 2518	Göschenen	688.910/170.000	granite
KAW 2608	Schw. Hörner	749.750/205.750	Verrucano conglomerate
KAW 2609	Sargans	755.150/212.750	sandstone
KAW 2612	Rothenbrunnen	752.400/181.148	Bündner schist
KAW 2616	Staldi	620.775/144.600	porphyritic biotite granite
KAW 2617	Niedergampel	621.150/129.200	muscovite-gneiss
KAW 2662	Lötschberg	621.050/144.200	granite
KAW 2663	Lötschberg	621.700/141.250	biotite-granite
KAW 2664	Lötschberg	622.150/139.300	granite
KAW 2702	Hockenhorn	623.700/141.525	biotite-granite
KAW 2703	Hockenhorn	623.490/141.950	biotite-gneiss
KAW 2761	Eggishorn	650.310/141.880	biotite-sericite-gneiss
KAW 2780	Wiwannihorn	632.470/133.050	granodiorite
KAW 2782	Baltschieder	632.949/128/330	sericite-biotite-augengneiss
KAW 2983	Ilanz	735.850/182.050	Verrucano conglomerate
KAW 3120	Fruttstock	703.430/180.260	biotite-amphibole-quartz monzonitic diorite
KAW 3121	Brunnibach	704.330/178.680	fine grained biotite-plagioclas gneiss
KAW 3123	Maderanertal	703.880/183.510	diatextite
KAW 3200	Scopi	708.800/159.200	granite
KAW 3215	Vättis	750.300/197.700	mylonite